Center for Turbulence Research
Proceedings of the Summer Program 2006

A quadrature-based moment closure for the Williams spray equation

By O. Desjardins, R. O. Fox† AND P. Villedieu‡

Sprays and other dispersed-phase systems can be described by a kinetic equation containing terms for spatial transport, acceleration, and particle processes (such as evaporation or collisions). In principle, the kinetic description is valid from the dilute (non-collisional) to the dense limit. However, its numerical solution in multi-dimensional systems is intractable due to the large number of independent variables. As an alternative, Lagrangian methods "discretize" the density function into "parcels" that are simulated using Monte-Carlo methods. While quite accurate, as in any statistical approach, Lagrangian methods require a relatively large number of parcels to control statistical noise, and thus are computationally expensive. A less costly alternative is to solve Eulerian transport equations for selected moments of the kinetic equation. However, it is well known that in the dilute limit, Eulerian methods have great difficulty describing correctly the moments as predicted by a Lagrangian method. A two-point quadrature-based Eulerian moment closure is developed and tested here for the Williams spray equation. It is shown that the method can successfully handle highly non-equilibrium flows (e.g., impinging particle jets, jet crossing, and particle rebound off walls) that heretofore could not be treated with the Eulerian approach.

1. Introduction

The direct quadrature method of moments (DQMOM) is an efficient Eulerian formulation for describing polydisperse multi-phase flows (Marchisio & Fox 2005). It is especially useful for treating dense sprays undergoing coalescence, and for submicron particulate/aerosol systems subject to Brownian aggregation (McGraw 1997; Marchisio *et al.* 2003). In comparison, standard moment methods have great difficulty treating systems with aggregation/coalescence and breakage. For other processes (e.g., evaporation, drag) the DQMOM equations are equivalent to the widely used Lagrangian particle method for sprays (Dukowicz 1980). However, even when used in this context, DQMOM has the inherent advantage over Lagrangian methods of precisely controlling the statistical noise in the lower-order moments (e.g., droplet number density, mass density, Sauter radius). For a given desired accuracy, this greatly reduces the computational cost since a large number of droplets is not required to eliminate statistical noise.

In previous work, the advantages of using DQMOM for treating particulate/aerosol populations with low Stokes numbers (i.e., the dispersed-phase velocity follows closely the velocity of the continuous phase) have been clearly demonstrated. These models have been implemented in flow codes for treating the formation of nanoparticles (e.g., soot), particles in flames, colloidal aggregation in liquids, and aerosols in the atmosphere. For these applications, the DQMOM transport equations take the form of standard scalar transport equations and are thus easily added to existing flow codes. The treatment of

† Chemical and Biological Engineering, Iowa State University
‡ ONERA, France

a dispersed phase with finite Stokes number introduces the additional complication of accounting for the dispersed-phase velocity (and its dependence on the particle size). In the Lagrangian formulation, this is done by solving for the particle velocity as it traverses the (Eulerian) gas phase. In quadrature methods, it is done by solving an Eulerian model where each quadrature node has it own velocity field.

In order to test the validity of the DQMOM for sprays, the laminar nozzle-flow problem described in Laurent *et al.* (2004) has been recently investigated (Fox *et al.* 2006) using both DQMOM and Lagrangian particle tracking. This problem is particularly challenging due to the significant coalescence rates caused by droplets of different sizes having very different Stokes numbers (and hence different velocities). Nevertheless, the comparison between the two methods showed excellent agreement between quantities such as the droplet number density, mass density, and Sauter radius. The computational cost for DQMOM was, however, two orders of magnitude lower than the Lagrangian method. This result is very promising and motivates our interest in developing the model further. The previous work on the DQMOM approach has identified two important points requiring further study (Fox *et al.* 2006): (1) the treatment of non-linear evaporation, and (2) the treatment of velocity dispersion in the context of moment closures. The second point was the topic investigated during the 2006 Summer Program; the principal results are reported here.

2. Quadrature-based moment closures

We will consider a laminar spray as an example of quadrature-based moment closures. The Williams equation (Williams 1958) for the joint volume (v), velocity ($\mathbf{u}$) number density function $f(v, \mathbf{u}; \mathbf{x}, t)$ is

$$\partial_t f + \mathbf{u} \cdot \partial_{\mathbf{x}} f + \partial_v \left(R_v f \right) + \partial_{\mathbf{u}} \cdot (\mathbf{F} f) = Q, \tag{2.1}$$

where R_v is the evaporation rate, $\mathbf{F}$ is the drag force acting on a droplet, and Q is the coalescence term. Note that the number density function has four degrees of freedom (one for v and three for $\mathbf{u}$), and it is intractable to solve directly using an Eulerian sectional method that discretizes v-$\mathbf{u}$ phase space. In most current applications (including the CTR spray code), Eq. 2.1 is approximated using a Lagrangian Monte-Carlo method (Dukowicz 1980). Although straightforward to implement numerically, this method does require a relatively large number of "parcels" to represent the spray in order to control statistical noise and bias. Note that extending f to include other variables (e.g., droplet temperature, chemical composition, etc.) is straightforward if the appropriate rate expressions are added to Eq. 2.1.

Classical moment closures for Eq. 2.1 start by defining the moments of f:

$$\langle v^k u_1^l u_2^m u_3^p \rangle \equiv \int_{-\infty}^{+\infty} \int_0^{\infty} v^k u_1^l u_2^m u_3^p f(v, \mathbf{u}) \, \mathrm{d}v \, \mathrm{d}\mathbf{u}, \tag{2.2}$$

where the usual practice is to consider only non-negative integers for k–p. Applying the moment transformation to Eq. 2.1 leads to a transport equation for the moments:

$$\partial_t \langle v^k u_1^l u_2^m u_3^p \rangle + \partial_{\mathbf{x}} \cdot \langle v^k u_1^l u_2^m u_3^p \mathbf{u} \rangle = \int_{-\infty}^{+\infty} \int_0^{\infty} v^k u_1^l u_2^m u_3^p P \, \mathrm{d}v \, \mathrm{d}\mathbf{u}, \tag{2.3}$$

where P denotes the terms for evaporation, drag, and coalescence. In general, only the first term in Eq. 2.3 is closed. The second term describes spatial transport and contains

moments one order higher in velocity:

$$\langle v^k u_1^l u_2^m u_3^p \mathbf{u} \rangle = \begin{bmatrix} \langle v^k u_1^{l+1} u_2^m u_3^p \rangle \\ \langle v^k u_1^l u_2^{m+1} u_3^p \rangle \\ \langle v^k u_1^l u_2^m u_3^{p+1} \rangle \end{bmatrix}, \tag{2.4}$$

and it is never closed. In contrast, the term on the right-hand side of Eq. 2.3 will be unclosed only when the rate expressions for evaporation, drag, and coalescence are nonlinear in v or $\mathbf{u}$. The closure of the right-hand side term using quadrature methods is investigated in detail elsewhere (Fox *et al.* 2006); the current focus will be on closures for the spatial transport term.

The DQMOM approximates the number density function by weighted delta functions in phase space (Fox 2003; Marchisio & Fox 2005):

$$f(v, \mathbf{u}) = \sum_{n=1}^{N} w_n \delta(v - v_n) \delta(\mathbf{u} - \mathbf{u}_n), \tag{2.5}$$

where $\delta(\mathbf{u} - \mathbf{u}_n) \equiv \delta(u_1 - u_{n1})\delta(u_2 - u_{n2})\delta(u_3 - u_{n3})$. Note that in this formulation, the weights w_n and abscissas (v_n, $\mathbf{u}_n$) are fields. The approximation in Eq. 2.5 is equivalent to the Lagrangian Monte-Carlo method. Thus we can interpret w_n to be the weights of parcels (w_n has units of number of droplets per unit volume), and v_n and $\mathbf{u}_n$ to be the corresponding volume and velocity, respectively. Application of DQMOM to Eq. 2.1 results in transport equations for the number density, mass density, and momentum density, respectively, of each quadrature node ($n = 1, \ldots, N$):

$$\partial_t w_n + \partial_{\mathbf{x}} \cdot (w_n \mathbf{u}_n) = a_n, \tag{2.6}$$

$$\partial_t (\rho_l w_n v_n) + \partial_{\mathbf{x}} \cdot (\rho_l w_n v_n \mathbf{u}_n) = \rho_l b_n + \rho_l w_n R_v(v_n, \mathbf{u}_n), \tag{2.7}$$

and

$$\partial_t (\rho_l w_n v_n \mathbf{u}_n) + \partial_{\mathbf{x}} \cdot (\rho_l w_n v_n \mathbf{u}_n \mathbf{u}_n) = \rho_l \mathbf{c}_n + \rho_l w_n \mathbf{u}_n R_v(v_n, \mathbf{u}_n) + \rho_l w_n v_n \mathbf{F}(v_n, \mathbf{u}_n), \tag{2.8}$$

where ρ_l is the liquid density, and a_n, b_n, and $\mathbf{c}_n$ are source terms due to coalescence (shown below) that are found from the right-hand side of Eq. 2.1. In principal, these equations can be solved with appropriate initial and boundary conditions to find the fields $w_n(\mathbf{x}, t)$ and ($v_n(\mathbf{x}, t)$, $\mathbf{u}_n(\mathbf{x}, t)$) appearing in Eq. 2.5. As described next, the choice of N determines how many moments can be controlled. In most applications, $2 \leq N \leq 4$ suffices to find results that agree well with the Lagrangian Monte-Carlo method (for which $100 < N$ parcels per grid cell is not uncommon).

The DQMOM approximation for the moments of the number density function is found directly from Eq. 2.5:

$$\langle v^k u_1^l u_2^m u_3^p \rangle = \sum_{n=1}^{N} w_n v_n^k u_{n1}^l u_{n2}^m u_{n3}^p. \tag{2.9}$$

The fundamental idea behind DQMOM is that we should choose the weights and abscissas such that as many moments as possible agree with moment transport equations found from Eq. 2.1. Note that there are a total of N weights and $4N$ abscissas and (equivalently) $5N$ unknown source terms in Eqs. 2.6–2.8. We will thus need to choose an equal number of independent moments to determine the source terms. The latter are found from a

linear system:

$$\sum_{n=1}^{N}(1-k)v_n^k u_{n1}^l u_{n2}^m u_{n3}^p a_n + \sum_{n=1}^{N}(k-l-m-p)v_n^{k-1}u_{n1}^l u_{n2}^m u_{n3}^p b_n + \sum_{n=1}^{N} v_n^{k-1}u_{n1}^l u_{n2}^m u_{n3}^p \left(l u_{n1}^{-1}c_{n1} + m u_{n2}^{-1}c_{n2} + p u_{n3}^{-1}c_{n3}\right) = P(k,l,m,p), \quad (2.10)$$

with the right-hand side depending only on the coalescence kernel (Fox *et al.* 2006). In the absence of coalescence (i.e., dilute systems), the solution to Eq. 2.10 is particularly simple: a_n, b_n, and $\mathbf{c}_n$ will be zero. In this limit, the right-hand sides of the DQMOM model (Eqs. 2.6–2.8) are the same as the Lagrangian model. Thus the left-hand sides tell us how to transform the Lagrangian model into an equivalent Eulerian representation. Finally, note that in the limit of small Stokes numbers, $\mathbf{u}_n$ can be replaced by the continuous-phase velocity and Eq. 2.8 is dropped. The DQMOM spray model then reduces to a set of scalar transport equations for w_n and v_n. However, our primary interest is the behavior of the quadrature model for finite Stokes numbers where $\mathbf{u}_n$ is not equal to the continuous-phase velocity.

3. Relation to multi-fluid models

Eulerian multi-fluid models describe polydisperse multi-phase flows by truncating the moments at low order. The most commonly employed multi-fluid models use the moments of order zero and one (which is equivalent to a one-point quadrature model):

$$\begin{bmatrix} n_p \\ n_p V_p \\ n_p V_p \mathbf{U}_p \end{bmatrix} = \begin{bmatrix} \langle 1 \rangle \\ \langle v \rangle \\ \langle v\mathbf{u} \rangle \end{bmatrix}, \quad (3.1)$$

where n_p is the number density, V_p is the average particle volume, and $\mathbf{U}_p$ is the average particle velocity. The model equations for these moments can be found from Eq. 2.3:

$$\partial_t n_p + \partial_{\mathbf{x}} \cdot \langle \mathbf{u} \rangle = \int_{-\infty}^{+\infty}\int_0^{\infty} P \,\mathrm{d}v\,\mathrm{d}\mathbf{u}, \quad (3.2)$$

$$\partial_t (n_p V_p) + \partial_{\mathbf{x}} \cdot \langle v\mathbf{u} \rangle = \int_{-\infty}^{+\infty}\int_0^{\infty} vP \,\mathrm{d}v\,\mathrm{d}\mathbf{u}, \quad (3.3)$$

$$\partial_t (n_p V_p \mathbf{U}_p) + \partial_{\mathbf{x}} \cdot \langle v\mathbf{u}\mathbf{u} \rangle = \int_{-\infty}^{+\infty}\int_0^{\infty} v\mathbf{u}P \,\mathrm{d}v\,\mathrm{d}\mathbf{u}. \quad (3.4)$$

However, because these equations are not closed, it is necessary to invoke a closure model. For example, it is usually assumed that $\langle v\mathbf{u} \rangle \approx n_p V_p \mathbf{U}_p$ and that $\langle v\mathbf{u}\mathbf{u} \rangle \approx n_p V_p \mathbf{U}_p \mathbf{U}_p + n_p V_p \boldsymbol{\sigma}^2$. The particle-velocity stress term $\boldsymbol{\sigma}^2$ must then be modeled to close the system. For the case of monodisperse particles (V_p constant) with P involving only linear drag (i.e., dilute systems without evaporation), the closed moment equations reduce to

$$\partial_t n_p + \partial_{\mathbf{x}} \cdot (n_p \mathbf{U}_p) = 0 \quad (3.5)$$

$$\partial_t (n_p \mathbf{U}_p) + \partial_{\mathbf{x}} \cdot (n_p \mathbf{U}_p \mathbf{U}_p) + \partial_{\mathbf{x}} \cdot (n_p \boldsymbol{\sigma}^2) = \kappa n_p (\mathbf{U}_f - \mathbf{U}_p)/St, \quad (3.6)$$

where κ is a drag coefficient, $\mathbf{U}_f$ is the fluid velocity, and St is the particle Stokes number.

In the limit of a small Stokes ($St \ll 1$), the particles will follow the fluid closely

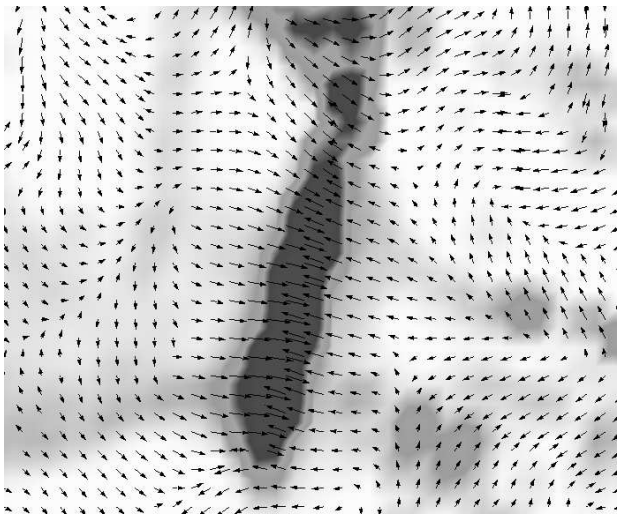

FIGURE 1. Particle velocity variance found from a Lagrangian simulation in isotropic turbulence with a finite Stokes number. Arrows indicate the direction of the most compressive strain rate of the fluid velocity. Regions of high variance are generated where the particles are unable to decelerate as quickly as the fluid. The multi-fluid model becomes unstable when the velocity variance is significant.

so that $\mathbf{U}_p \approx \mathbf{U}_f$. In this limit, it is possible to set $\boldsymbol{\sigma}^2$ equal to zero and Eq. 3.6 becomes the pressureless gas dynamics equation. If $\boldsymbol{\sigma}^2$ is neglected for a finite Stokes ($0 < St$), the pressureless gas dynamics equation will be ill-posed. Physically, this ill-posedness is a result of particle-trajectory crossings. In other words, at finite Stokes there is a non-zero probability that two particles located at the same point in space will have different velocities. An example of this behavior in illustrated in Fig. 1. In fact, in highly non-equilibrium flows the velocity density function can be locally bimodal (e.g., particles traveling in opposite directions) while closures employed in multi-fluid models always assume monomodal density functions (e.g., joint Gaussian). Physically, particle-trajectory crossings imply that the particle-velocity stress term becomes non-zero at finite Stokes. Indeed, setting $\boldsymbol{\sigma}^2 > 0$ will help to stabilize Eq. 3.6; however, it will not be sufficient to remove singularities for finite Stokes numbers (e.g., $St \approx 1$). As shown in Fig. 2 (other examples are shown in Section 6), Eulerian moment closures based on neglecting $\boldsymbol{\sigma}^2$ do not agree with Lagrangian simulations for even the simplest non-equilibrium flows. Thus, in this work we propose an alternative closure based on two-point quadrature.

4. A two-point quadrature closure

Because the trajectory-crossing problem occurs due to initial/boundary conditions or to the drag term, we need not consider the effects of evaporation and coalescence when developing a closure for the velocity moments. We will therefore limit our attention here to dilute systems with linear drag and monodisperse particles. The two-point quadrature approximation for the velocity moments for this case is

$$\langle u_1^l u_2^m u_3^p \rangle = w_1 u_{11}^l u_{12}^m u_{13}^p + w_2 u_{21}^l u_{22}^m u_{23}^p, \tag{4.1}$$

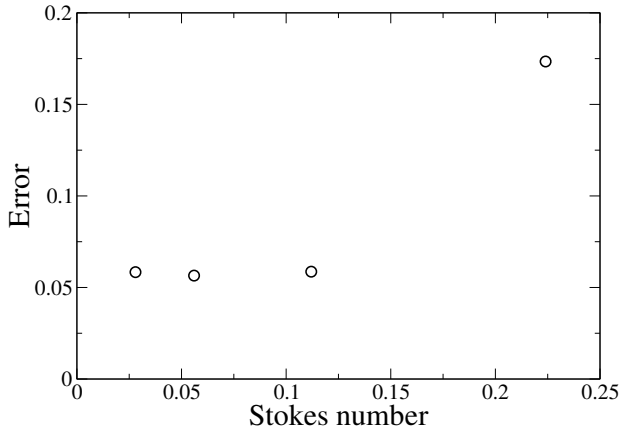

FIGURE 2. Error between the velocity fields computed by the Eulerian multi-fluid model and the Lagrangian method. At a finite Stokes number the error increases significantly as particle-trajectory crossings become significant. For larger Stokes numbers, the Eulerian code is numerically unstable due to singularities in the number density field. Although singularities can be "smoothed" by adding artificial viscosity, none of the velocity moments will be accurately predicted for finite Stokes numbers.

where w_n and $\mathbf{u}_n$ are the weights and velocity abscissas, respectively. Note that the weights and abscissas represent $2+2d$ unknowns for a d-dimensional system. It will thus be necessary to choose an equal number of moments to close the system. In this work we use the following set of $2+2d$ moments ($i=1,\ldots,d$):

$$\begin{gathered} m_0 = \langle 1 \rangle = w_1 + w_2, \quad m_{1i} = \langle u_i \rangle = w_1 u_{1i} + w_2 u_{2i}, \\ m_{2i} = \langle u_i^2 \rangle = w_1 u_{1i}^2 + w_2 u_{2i}^2, \quad Q = \sum_{i=1}^{d} \langle u_i^3 \rangle = \sum_{i=1}^{d} \left(w_1 u_{1i}^3 + w_2 u_{2i}^3 \right). \end{gathered} \tag{4.2}$$

(Note that $n_p = m_0$, $n_p U_{pi} = m_{1i}$, and $n_p \sigma_{ii}^2 = m_{2i} - n_p U_{pi}^2$.) This system of non-linear equations can be solved to find the weights and abscissas in terms of the moments:

$$\begin{gathered} w_1 = (1/2 + \alpha) m_0, \quad w_1 = (1/2 - \alpha) m_0, \\ u_{1i} = U_{pi} - (w_2/w_1)^{1/2} \sigma_{ii}, \quad u_{2i} = U_{pi} + (w_1/w_2)^{1/2} \sigma_{ii}, \end{gathered} \tag{4.3}$$

with

$$\alpha = \frac{q_p/2}{\left(q_p^2 + 4 \left(\sum_{i=1}^{d} \sigma_{ii}^3 \right)^2 \right)^{1/2}} \tag{4.4}$$

where

$$q_p = Q/m_0 - \sum_{i=1}^{d} U_{pi}^3 - 3 \sum_{i=1}^{d} \sigma_{ii}^2 U_{pi}. \tag{4.5}$$

Thus, knowledge of the values of the moments in Eq. 4.2 is equivalent to knowledge of the values of the weights and abscissas. Also note that the weights and abscissas can then be used in Eq. 4.1 to approximate any desired moment.

The transport equations for the set of the moments in Eq. 4.2 in the dilute limit follow

from Eq. 2.3:

$$\partial_t m_0 + \partial_{x_j} m_{1j} = 0, \tag{4.6}$$

$$\partial_t m_{1i} + \partial_{x_j} m_{2ji} = \kappa(U_{fi} m_0 - m_{1i})/St, \tag{4.7}$$

$$\partial_t m_{2i} + \partial_{x_j} m_{3ji} = 2\kappa(U_{fi} m_{1i} - m_{2i})/St, \tag{4.8}$$

$$\partial_t Q + \partial_{x_j} m_{4j} = 3\kappa \sum_{i=1}^{d} (U_{fi} m_{2i} - m_{3i})/St, \tag{4.9}$$

where summation is implied over repeated indices. The spatial transport terms in these equations are closed by writing them in terms of the weights and abscissas:

$$m_{2ji} = \langle u_j u_i \rangle = w_1 u_{1j} u_{1i} + w_2 u_{2j} u_{2i}, \tag{4.10}$$

$$m_{3ji} = \langle u_j u_i^2 \rangle = w_1 u_{1j} u_{1i}^2 + w_2 u_{2j} u_{2i}^2, \tag{4.11}$$

$$m_{4j} = \sum_{i=1}^{d} \langle u_j u_i^3 \rangle = \sum_{i=1}^{d} \left(w_1 u_{1j} u_{1i}^3 + w_2 u_{2j} u_{2i}^3 \right). \tag{4.12}$$

If the fluid velocity $\mathbf{U}_f$ is known, then the moment transport equations (4.6–4.9) are closed and can be solved numerically to find the moments in Eq. 4.2 (or equivalently the weights and abscissas). Finally, we can note that two-point quadrature closes the system of velocity moments at third order, while the multi-fluid model attempts to close at first (or second) order. We shall see that this higher-order closure greatly improves the predictive capabilities of the quadrature-based moment closure.

5. Numerical scheme

The numerical scheme used to solve Eqs. 4.6–4.9 employs a kinetic transport scheme to evaluate the spatial fluxes. Considering a one-dimensional system, the moment equations become

$$\partial_t m_0 + \partial_x m_1 = 0, \tag{5.1}$$

$$\partial_t m_1 + \partial_x m_2 = \kappa(U_f m_0 - m_1)/St, \tag{5.2}$$

$$\partial_t m_2 + \partial_x m_3 = 2\kappa(U_f m_1 - m_2)/St, \tag{5.3}$$

$$\partial_t m_3 + \partial_x m_4 = 3\kappa(U_f m_2 - m_3)/St, \tag{5.4}$$

where $Q = m_3$. A first-order, explicit, finite-volume scheme for these equations can be written for the set of moments $m = [m_0\, m_1\, m_2\, m_3]^{\mathrm{T}}$ as

$$m_i^{n+1} = m_i^n - \frac{\Delta t}{\Delta x} \left[G(m_i^n, m_{i+1}^n) - G(m_{i-1}^n, m_i^n) \right] + \Delta t S_i^n \tag{5.5}$$

where n is the time step, i is the grid node, S is the drag term, and G is the flux function. Using the velocity abscissas, we can determine whether a quadrature node is moving left to right, or right to left. The flux function can then be expressed as

$$G(m_i, m_{i+1}) = H^+(m_i) + H^-(m_{i+1}) \tag{5.6}$$

where

$$H^+(m_i) = \max(u_{1i}, 0) \begin{bmatrix} w_{1i} \\ w_{1i}u_{1i} \\ w_{1i}u_{1i}^2 \\ w_{1i}u_{1i}^3 \end{bmatrix} + \max(u_{2i}, 0) \begin{bmatrix} w_{2i} \\ w_{2i}u_{1i} \\ w_{2i}u_{1i}^2 \\ w_{2i}u_{1i}^3 \end{bmatrix},$$
$$H^-(m_i) = \min(u_{1i}, 0) \begin{bmatrix} w_{1i} \\ w_{1i}u_{1i} \\ w_{1i}u_{1i}^2 \\ w_{1i}u_{1i}^3 \end{bmatrix} + \min(u_{2i}, 0) \begin{bmatrix} w_{2i} \\ w_{2i}u_{1i} \\ w_{2i}u_{1i}^2 \\ w_{2i}u_{1i}^3 \end{bmatrix}. \tag{5.7}$$

The extension of this flux function to two- and three-dimensional systems is straightforward using the normal vectors on the faces of the finite-volume cells to determine the direction of motion for each quadrature node. Although not done so here, it is also possible to derive higher-order schemes for the flux function. The key point in all cases is that the quadrature method provides a realizable set of weights and abscissas at every grid node that can be used to determine the node velocities. This is not possible with other moment closures (such as the multi-fluid model). In the context of two-point quadrature, particle-trajectory crossing can be interpreted as u_1 and u_2 having different signs at the same grid point.

6. Results and discussion

In this section we apply the quadrature-based closure to three non-equilibrium particle flows in order to illustrate its ability to handle non-trivial problems. Because the drag term offers no particular closure problem (see Eqs. 4.6–4.9), for clarity we will consider cases without drag (or equivalently infinite Stokes number). However, we should emphasize that the quadrature-based closure has been found to work satisfactorily over the entire range of Stokes numbers.

6.1. *One-dimensional impinging particles*

The first flow that we consider is one-dimensional with two particle "packets" moving in opposite directions. The initial number density n_p is shown in Fig. 3 ($t = 0$), where it can be seen that the packet on the left has number density one-half as large as that on the right. The initial average particle velocity U_p is set to 1 for $x < 0.5$ and -1 for $x \geq 0.5$. The two packets will thus eventually collide. In terms of the moments, the initial conditions are

$$m_0 = n_p,\ m_1 = n_p U_p,\ m_2 = n_p,\ m_3 = n_p U_p,$$

which yields the following weights and abscissas for two-point quadrature:

$$w_1 = n_p/2,\ w_2 = n_p/2,\ u_1 = U_p,\ u_2 = U_p.$$

We then applied the numerical scheme described in Section 5 to advance the moments for both the standard (one-point) moment closure and the two-point quadrature closure.

Figure 3 illustrates the resulting time evolution of the number density. Before collision (i.e., before n_p at $x = 0.5$ is greater than machine precision) both the standard and two-point quadrature moment closures yield identical results for n_p. However, as soon as n_p becomes non-zero at $x = 0.5$ the two closures predict different values for all of the moments. With the standard moment closure n_p accumulates at $x = 0.5$ (i.e., the particles become completely segregated from the fluid) and the average velocity U_p is independent

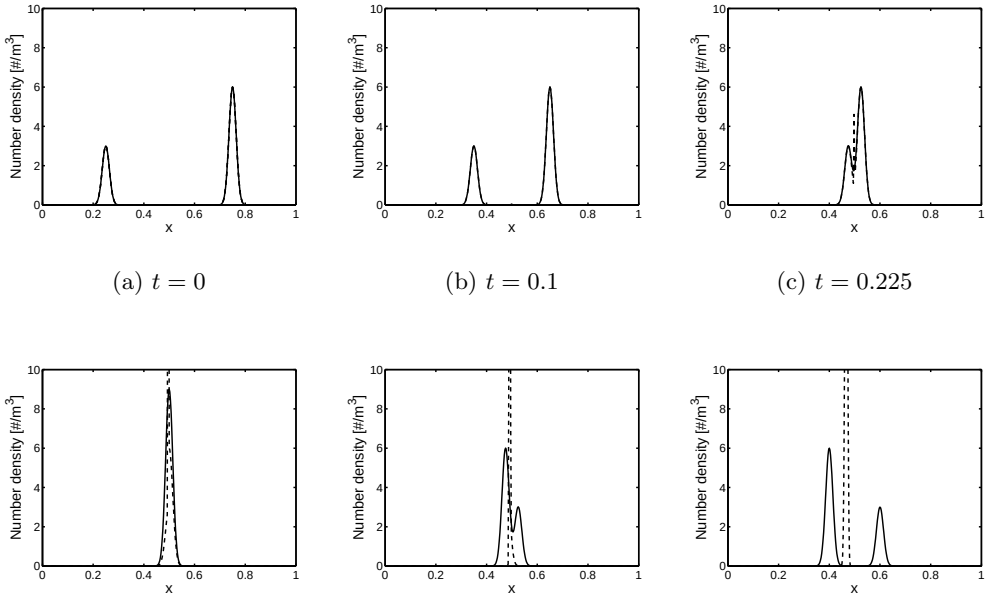

(a) $t = 0$ (b) $t = 0.1$ (c) $t = 0.225$

(d) $t = 0.25$ (e) $t = 0.275$ (f) $t = 0.35$

FIGURE 3. Number density for one-dimensional impinging particles for six different times. ——, two-point quadrature closure; – –, standard moment closure.

of t. In contrast, with the two-point quadrature closure the two packets pass through each other and the average velocity (not shown) evolves in a non-trivial manner to finally end at U_p equal -1 for $x < 0.5$ and 1 for $x \geq 0.5$ (i.e., the opposite sign compared to the initial conditions). As mentioned earlier, the dramatic differences between the two closures is due to the fact that two-point quadrature can describe particle-crossing trajectories, while the standard moment closure cannot. Without this ability, a moment closure cannot predict any of the velocity moments (including the zero-order moment) correctly for finite Stokes numbers. This fact has important ramifications on the validity of using Eulerian multi-fluid models to investigate particle segregation in dilute fluid-particle flows (e.g., Kaufmann *et al.* 2006). This simple example shows that in general the segregation levels predicted by the standard moment closure will be much larger than what would be found using a Lagrangian method.

6.2. *Crossing particle jets*

In this example, we demonstrate the ability of the two-point quadrature closure to capture particle-crossing trajectories in two-dimensional flows. The flow domain is the unit square and particle jets are introduced centered at the bottom and right-hand sides of the domain with equal velocities (see Fig. 4). The evolution of the particle number density is shown in Fig. 4. At early times the jets advance toward the center point. At $t = 0.9$, the jets begin to overlap and the local number density doubles. For subsequent times, the jets continue along their original trajectories and finally exit the flow domain at the top and left-hand sides, respectively. Note that if the standard moment closure were used to compute this flow, the jets would "collide" at the center point and move off diagonally in one stream

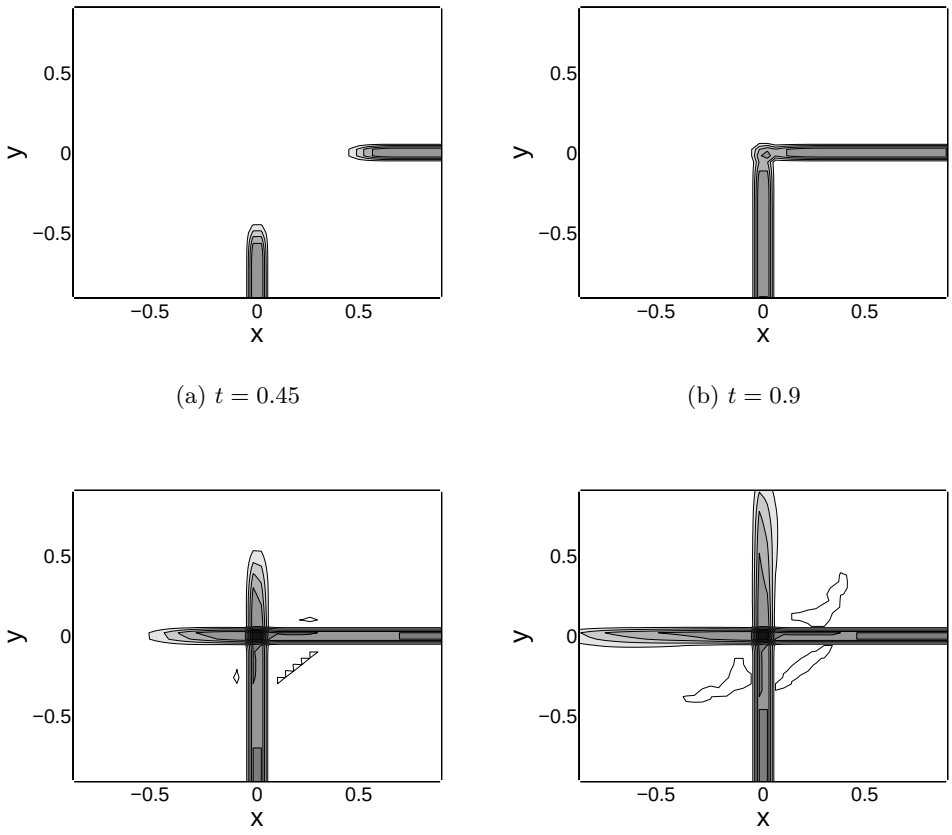

(a) $t = 0.45$ (b) $t = 0.9$

(c) $t = 1.35$ (d) $t = 1.8$

FIGURE 4. Particle number density for crossing jets for four different times.

toward the upper left-hand corner of the domain. Finally, we can note that because the numerical scheme is first order, numerical dispersion is observed at the leading edges of the jets. In principle, this numerical artifact could be diminished by using a higher-order scheme. Just as in the previous example, the key to success is the fact that two-point quadrature can describe the bimodal velocity distribution that occurs in the jet-overlap region near the center point. Indeed, in the overlap region the two velocity abscissas have values $\mathbf{u}_1 = [0\,1]^{\mathrm{T}}$ and $\mathbf{u}_2 = [-1\,0]^{\mathrm{T}}$, which correspond to the average velocity boundary condition on the lower and right-side walls, respectively.

6.3. *Particle-wall rebound*

In the final example, we consider a particle jet rebounding off a reflective wall. In this flow, the particle jet enters through the left-hand side of the domain with average velocity $U_p = [1\ -1]^{\mathrm{T}}$ (see Fig. 5). The jet proceeds toward the bottom reflecting wall, where it is reflected back into the box before exiting from the left-hand side. The boundary condition along the bottom wall is straightforward to implement in terms of the velocity abscissas. We simply change the y component of the node velocities as follows: $\mathbf{u}_{n2} \rightarrow -e\mathbf{u}_{n2}$ where

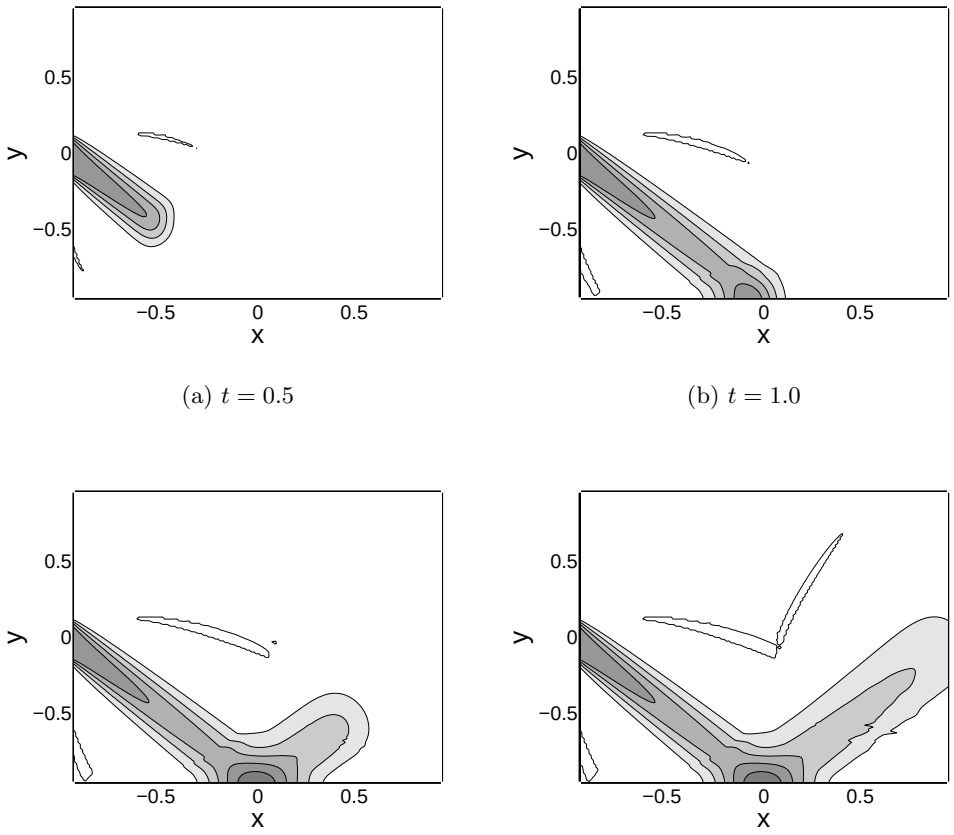

(a) $t = 0.5$ (b) $t = 1.0$

(c) $t = 1.5$ (d) $t = 2.0$

FIGURE 5. Particle number density for particle-wall rebound for four different times.

$e = 1$ is the coefficient of restitution. Thus, one can easily simulate particle rebounds off partially reflective walls by choosing $0 < e < 1$. Note that in this example, the particle velocity is bivariate near the impingement point at the wall due to the incoming velocity of $[1\ {-1}]^{\mathrm{T}}$ and the outgoing velocity of $[1\ e]^{\mathrm{T}}$. The average velocity just above the wall is therefore $[1\ (e-1)/2]^{\mathrm{T}}$. Because the standard moment closure uses the average velocity for convective transport, it is not able to reflect particles from the wall. Once again, the two-point quadrature closure overcomes this difficulty in an intuitive and straightforward manner. Finally, Fig. 5 illustrates the idea that the numerical dispersion is significantly larger for this example, which is essentially due to the fact that the jet travels at a 45° angle to the grid lines. As noted previously, the quality of the simulations could be improved by using a higher-order numerical scheme for convective transport. Nevertheless, the three examples presented here clearly demonstrate the power of quadrature-based moment closures to represent the dynamics of non-equilibrium particle flows.

7. Conclusions

A two-point quadrature-based moment closure for the Williams spray equation has been derived and verified for one- and two-dimensional, non-equilibrium, dilute, particle flows. In contrast to the "standard" Eulerian multi-fluid (or one-point) model, the two-point quadrature closure can successfully handle flows with particle-crossing trajectories and thus is able to compute accurately the lower-order velocity moments previously obtainable only by employing a Lagrangian method. While further work is needed to extend the quadrature method to higher orders (e.g., three-point quadrature) and three-dimensional flows, the ability to compute accurate particle velocity statistics (including, for example, particle energy spectra) in an Eulerian framework should make the quadrature-based models very attractive for many applications involving dispersed-phase flows.

Acknowledgment

ROF gratefully acknowledges support from U.S. National Science Foundation.

REFERENCES

Dukowicz, J. K. 1980 A particle-fluid numerical model for liquid sprays. *J. Comp. Phys.* **35** (2), 229–253.

Fox, R. O. 2003 *Computational Models for Turbulent Reacting Flows*. Cambridge: Cambridge University Press.

Fox, R. O., Laurent, F. & Massot, M. 2006 Numerical simulation of polydisperse, dense liquid sprays in an Eulerian framework: direct quadrature method of moments and multi-fluid method. *J. Comp. Phys. submitted*.

Kaufmann, A., Simonin, O. & Poinsot, T. 2004 Direct numerical simulation of particle-laden homogeneous isotropic turbulent flows using a two-fluid model formulation. In *Proceedings of 5th International Conference on Multiphase Flow (ICMF'04)*.

Laurent, F., Massot, M. & Villedieu, P. 2004 Eulerian multi-fluid modeling for the numerical simulation of polydisperse dense liquid spray. *J. Comp. Phys.* **194**, 505–543.

Marchisio, D. L. & Fox, R. O. 2005 Solution of population balance equations using the direct quadrature method of moments. *J. Aerosol. Sci.* **36**, 43–73.

Marchisio, D. L., Vigil, R. D. & Fox, R. O. 2003 Quadrature method of moments for aggregation-breakage processes. *J. Colloid Interface Sci.* **258** (2), 322–334.

McGraw, R. 1997 Description of aerosol dynamics by the quadrature method of moments. *Aerosol Sci. Tech.* **27**, 255–265.

Williams, F. A. 1958 Spray combustion and atomization. *Phys. Fluids* **1**, 541–545.